



Fig. 1. Ellipsoidal representation of the conformation of a coiled polyion.

-  : Represents a condensed counterion
-  : Represents a free counterion (in the ionic atmosphere)

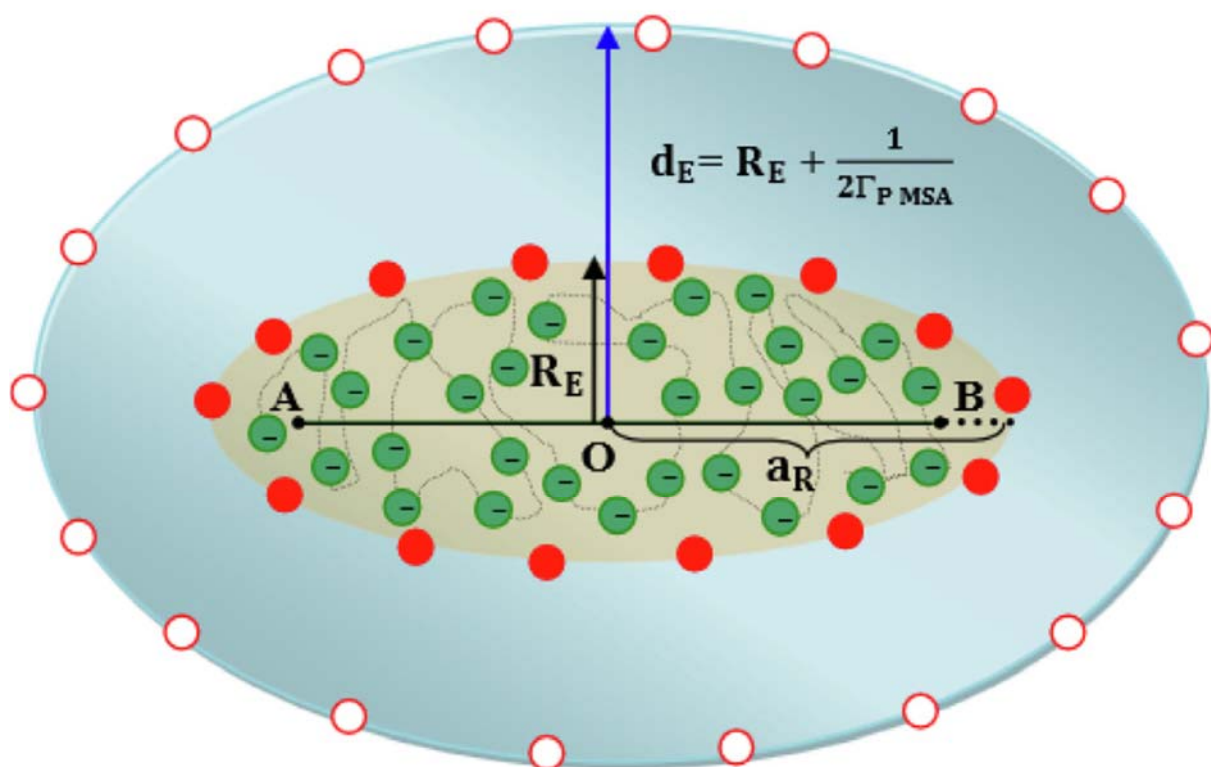


Fig. 2. Representation of an ellipsoidal polyion surrounded by its condensed counterions and its ionic atmosphere.

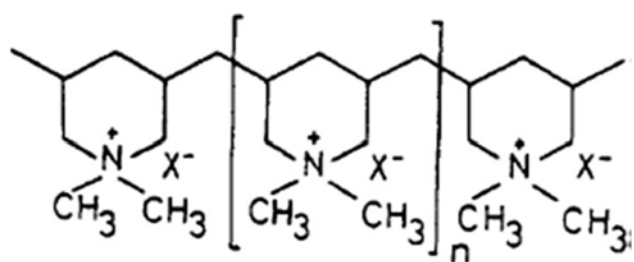


Fig. 3 Expanded formula of poly(1,1-dimethyl-3,5-dimethylene piperidinium) PDDP^{Zs+} polyion chain.

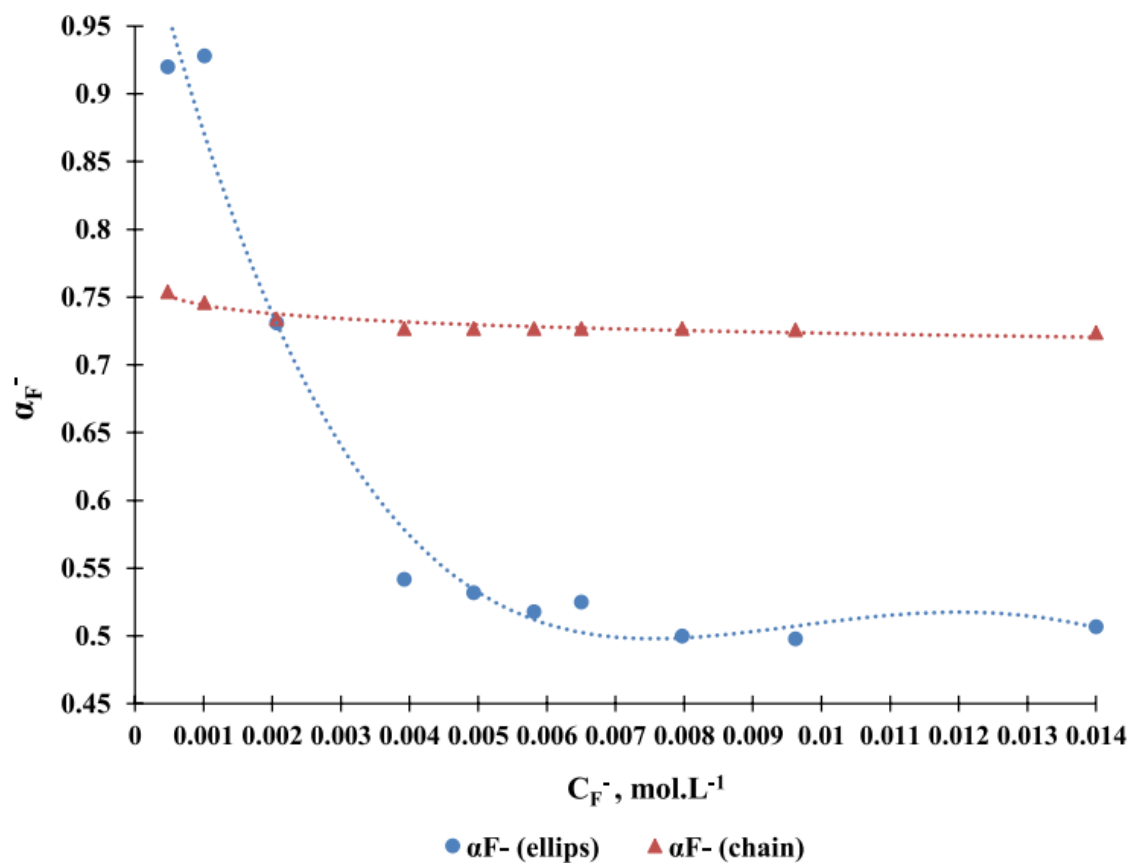
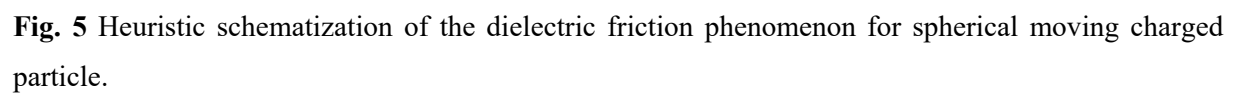


Fig. 4 Comparison between the theoretical variations with the counter ion concentration C_F^- , of the degree of dissociation α_F^- in the case of ellipsoidal model and in the case of stretched chain model, for PDDPF polyelectrolytes in aqueous solution at 25 °C.



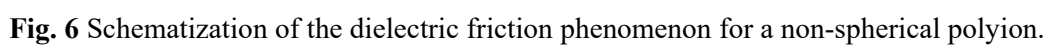


Fig. 6 Schematization of the dielectric friction phenomenon for a non-spherical polyion.

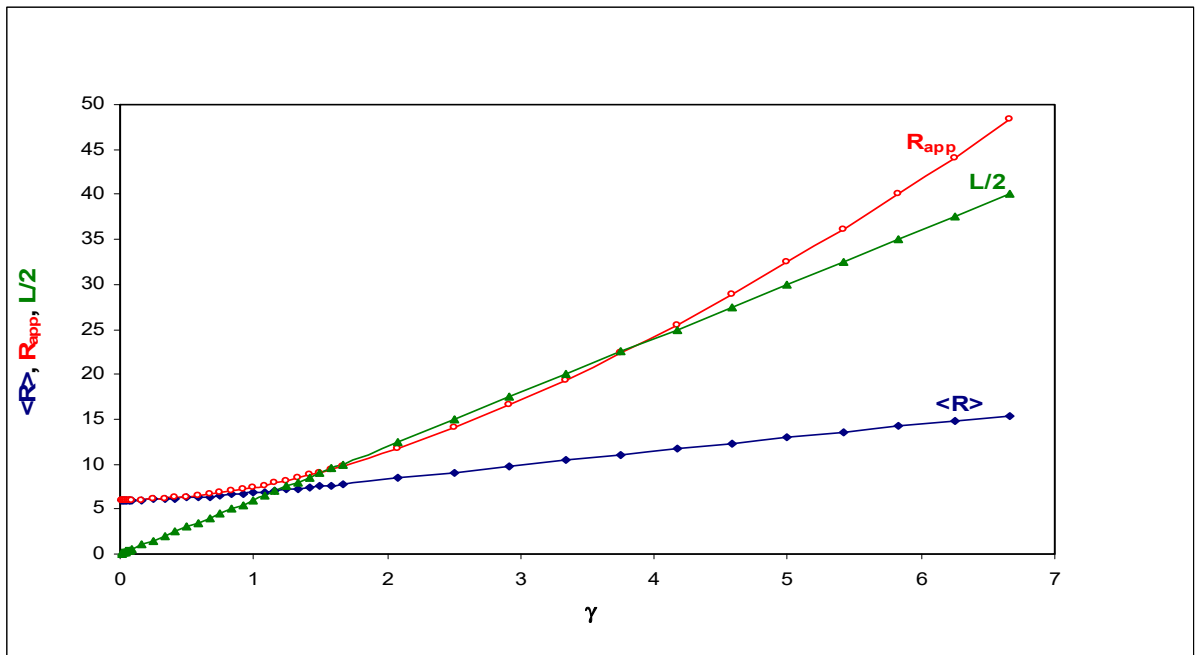


Fig. 7 Comparison of the variations of the apparent radius R_{app} , the inter-foci distance L and the mean radius $\langle R \rangle$ of an ellipsoidal polyion with its eccentricity $\gamma = L/2R$.

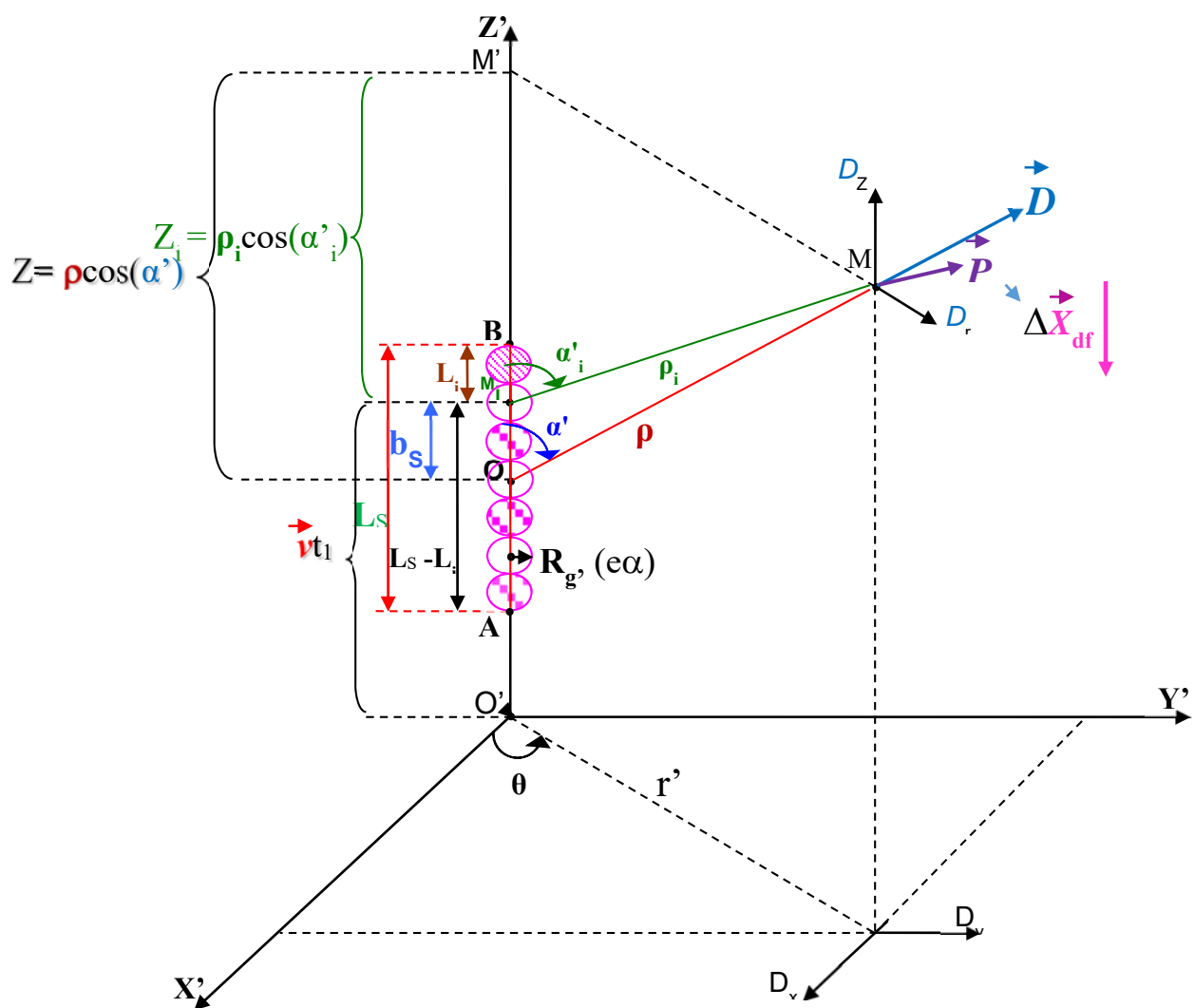


Fig. 8 Schematization of the dielectric friction phenomenon for a chain of successive charged spheres.

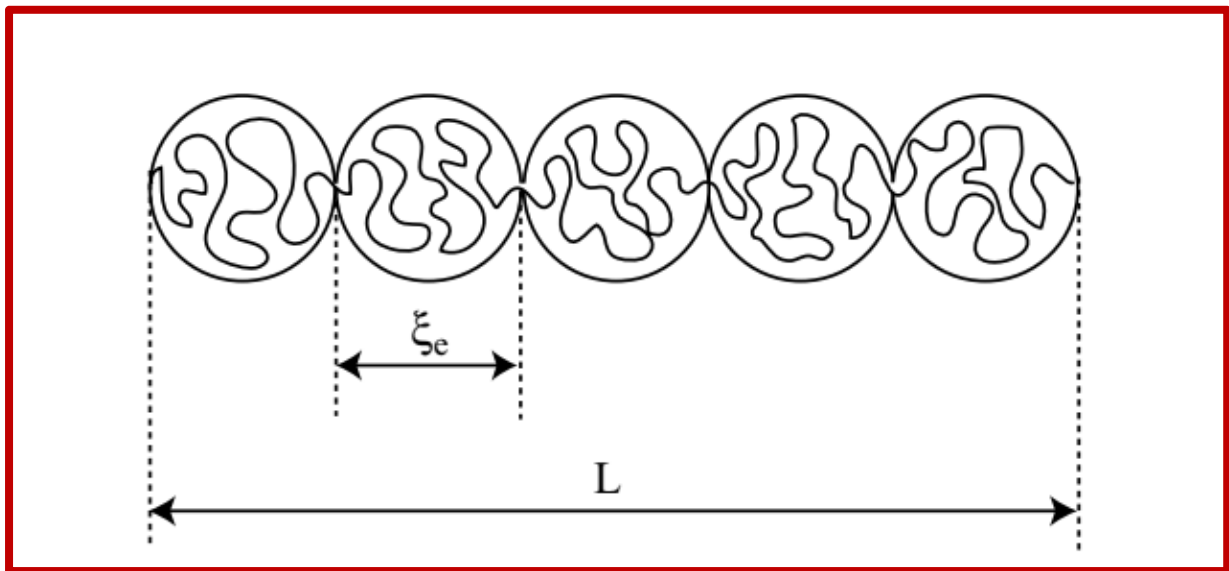


Fig. 9. Representation of a moving polyion as a chain of successive charged electrostatic blobs.

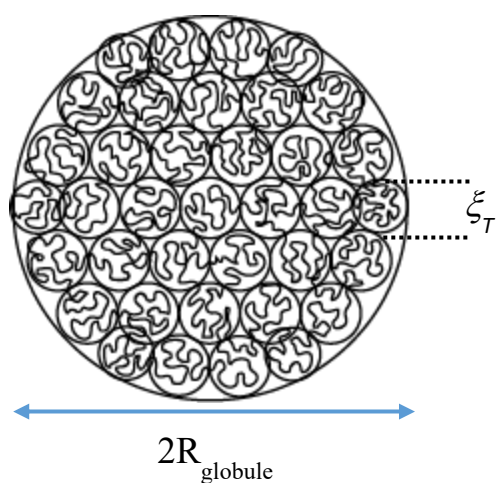


Fig. 10 Globular hydrophobic Polymer represented as dense stack of Thermal Blobs of size ξ_T .

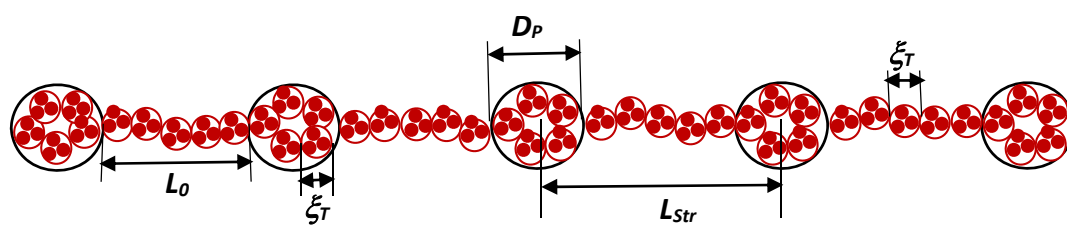


Fig. 11 The "pearl necklace" conformation of a hydrophobic polyion chain.

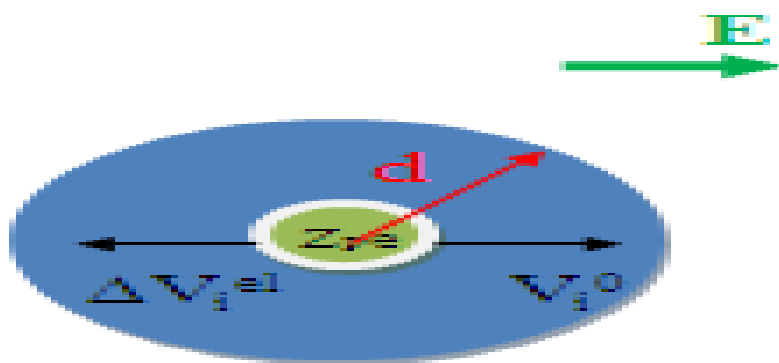


Fig. 12 Schematization of the electrophoretic effect undergone by a moving polyion.

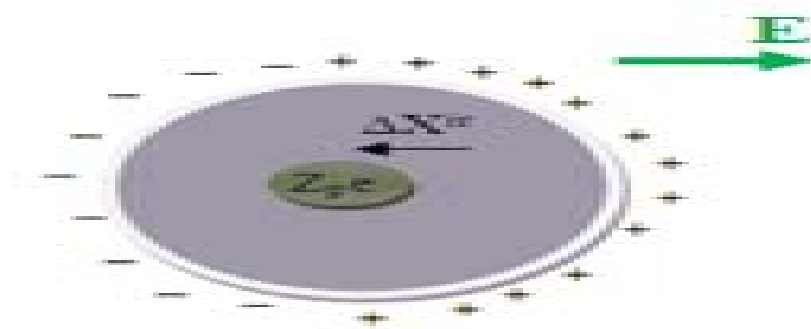


Fig. 13 Schematization of the ionic relaxation friction undergone by a moving polyion.

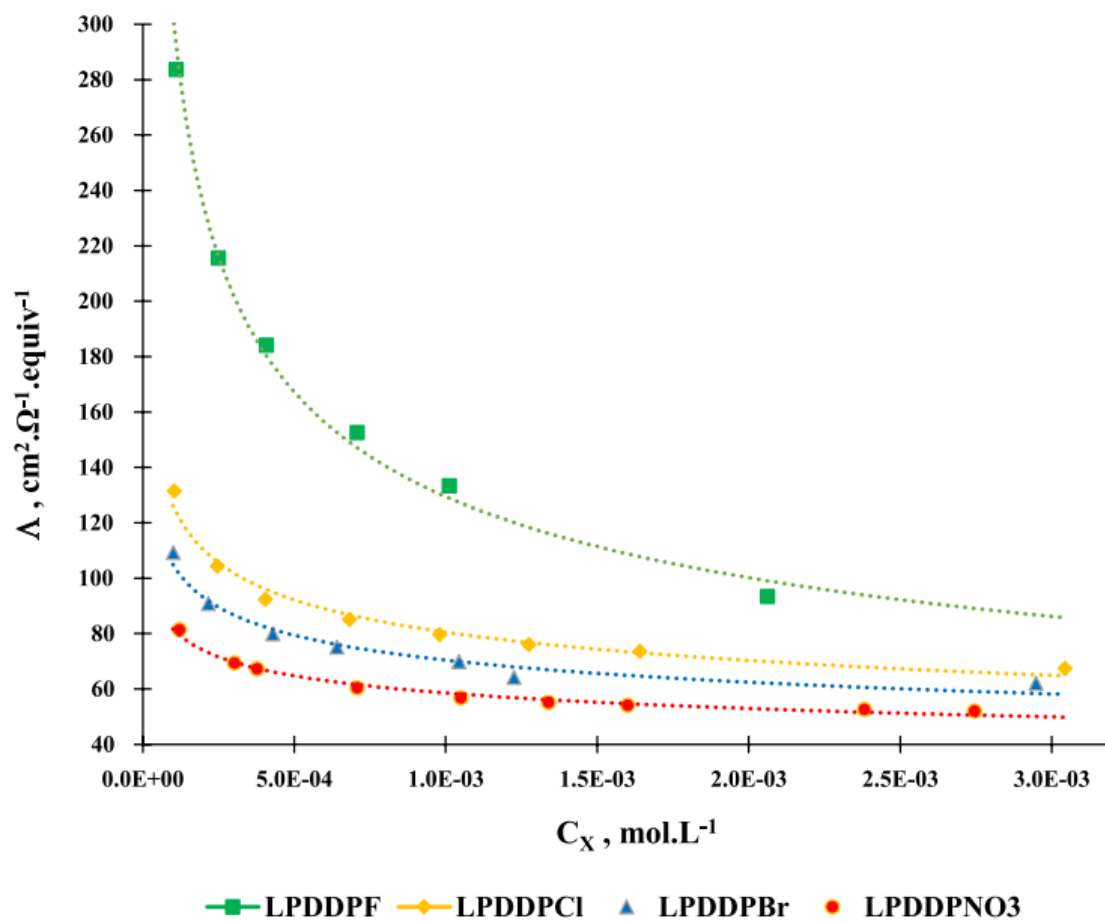


Fig. 14 Variations with the ionic concentration C_X of experimental equivalent conductivities: $\Lambda^{\text{exp}}_{\text{PDDPF}}$, $\Lambda^{\text{exp}}_{\text{PDDPCI}}$, $\Lambda^{\text{exp}}_{\text{PDDPBr}}$ and $\Lambda^{\text{exp}}_{\text{PDDPNO}_3}$, of PDDPX polyelectrolytes in water at 25°C.

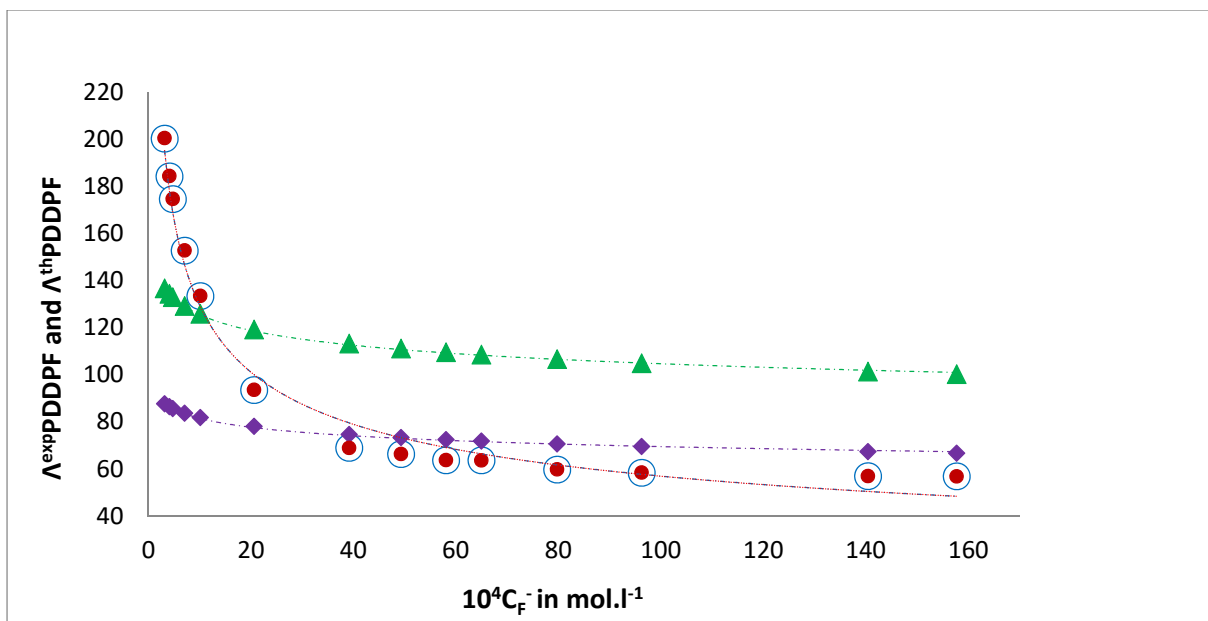


Fig. 15 Comparison of the variations with concentration C_F^- of the equivalent conductivities $\Lambda^{\text{Manning,cor}}_{\text{PDDPF}}$, $\Lambda^{\text{Colby}}_{\text{PDDPF}}$, $\Lambda^{\text{exp}}_{\text{PDDPF}}$, $\Lambda^{\text{th}}_{\text{PDDPF}}$, respectively of Manning, Colby, experimental, and ours theoretical Conductibility, of Fluoride poly(1,1-dimethyl-3,5-dimethylene piperidinium) PDDPF polyelectrolyte.

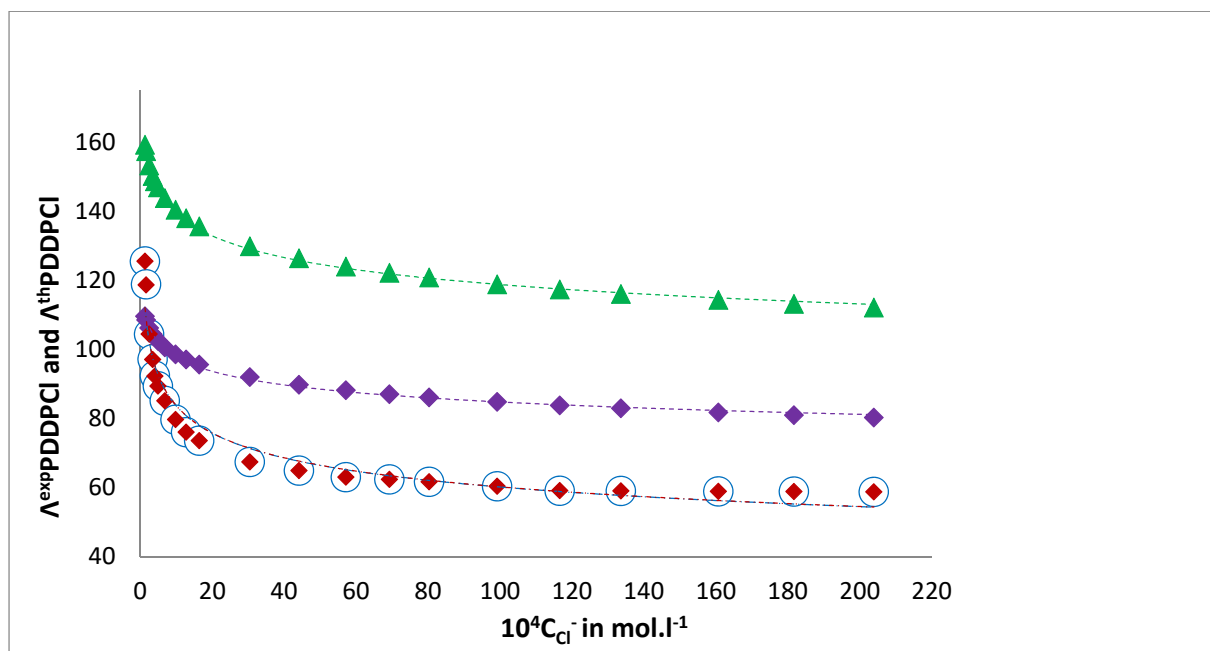


Fig. 16 Comparison of the variations with concentration C_{Cl^-} of the equivalent conductivities $\Lambda^{Manning,cor}_{PDDPCL}$, Λ^{Colby}_{PDDPCL} , Λ^{exp}_{PDDPCL} , Λ^{th}_{PDDPCL} , respectively of Manning, Colby, experimental, and ours theoretical Conductibility, of Chloride poly(1,1-dimethyl-3,5-dimethylene piperidinium) PDDPCL polyelectrolyte.

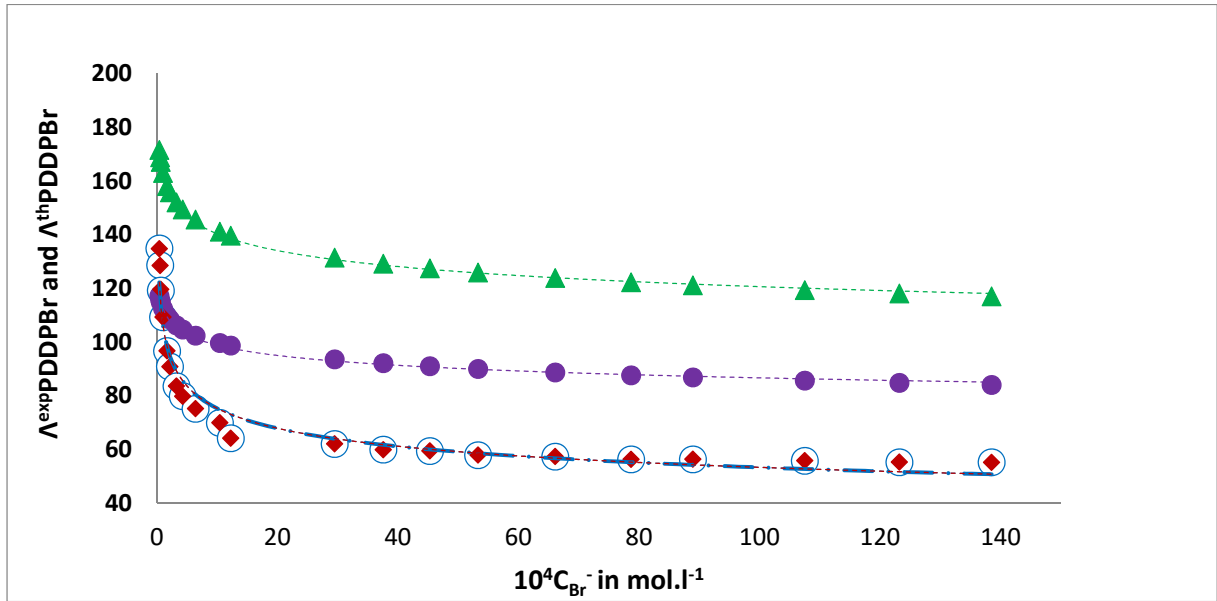


Fig. 17 Comparison of the variations with concentration C_{Br^-} of the equivalent conductivities $\Lambda^{Manning,cor}_{PDDPBr}$, Λ^{Colby}_{PDDPBr} , Λ^{exp}_{PDDPBr} , Λ^{th}_{PDDPBr} , respectively of Manning, Colby, experimental, and ours theoretical Conductibility, of Bromide poly(1,1-dimethyl-3,5-dimethylene piperidinium) PDDPBr polyelectrolyte.

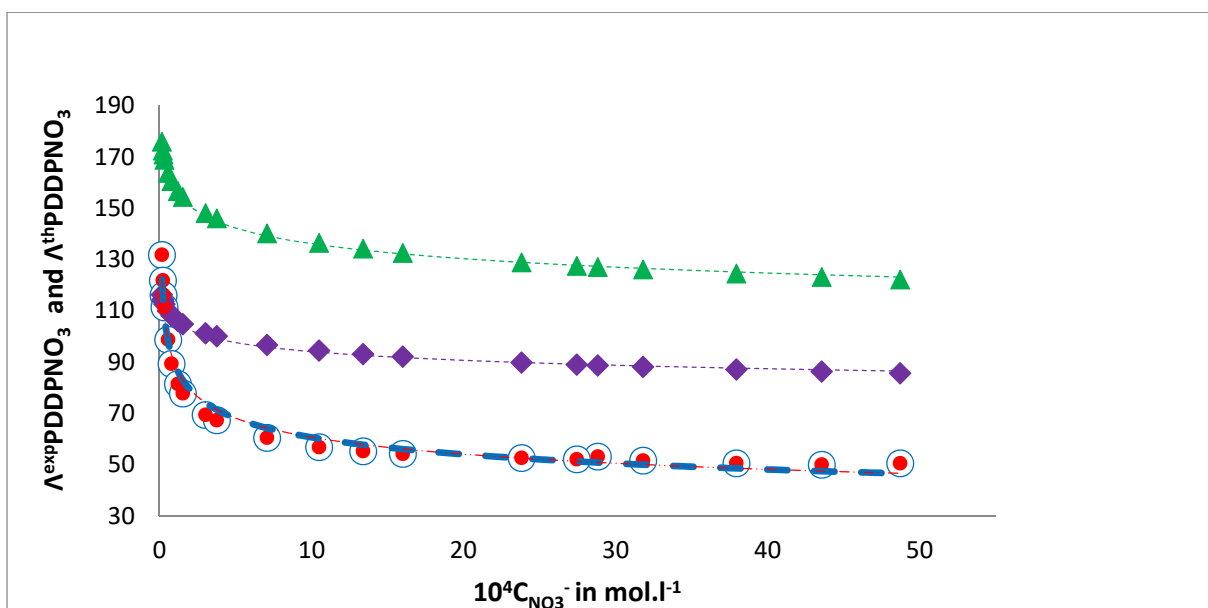


Fig. 18 Comparison of the variations with concentration $C_{NO_3^-}$ of the equivalent conductivities $\Lambda^{Manning,cor}_{PDDPNO_3}$, $\Lambda^{Colby}_{PDDPNO_3}$, $\Lambda^{exp}_{PDDPNO_3}$, $\Lambda^{th}_{PDDPNO_3}$, respectively of Manning, Colby, experimental, and ours theoretical Conductibility, of Nitrate poly(1,1-dimethyl-3,5-dimethylene piperidinium) PDDPNO₃ polyelectrolyte.